Submitted to *Nature*, July 15, 2003.

Supplementary Information

Cooling history of the Pacific lithosphere

Michael H. Ritzwoller, Nikolai M. Shapiro, & Shi-Jie Zhong

Department of Physics, University of Colorado at Boulder, Boulder, CO 80309-0390 USA

Data coverage, expressed as path density of Rayleigh wave group velocities, is shown in Figure 1. Coverage is best at intermediate periods, and reduces particularly at very long periods. It is also considerably lower for Love waves than for Rayleigh waves, especially at periods above about 100 sec. Resolution estimates are shown in Figure 2. Average resolution across the Pacific is about 600 km at 20 sec, 720 km at 50 sec, 850 km at 100 sec, and 980 km at 150 sec period.

Examples of 50 sec dispersion maps are presented in Figure 3 for Rayleigh wave group and phase velocity and Love wave group velocity. The trends are similar to those discussed for the shear velocity and temperature models in the main text. There is a general increase in wave speed toward the western Pacific, consistent with the prediction for a diffusively cooling half-space (Half-Space Cooling or HSC model). As Figure 3g-3i show, 50 sec surface wave dispersion is in remarkable agreement with the predictions from the HSC model up to about 70 Ma, but a systematic deviation from the HSC model sets on in the Central Pacific at lithospheric ages that range from about 70 Ma to somewhat more than 100 Ma. These trends are both period and wave type dependent, but are summarized in 3-D seismic model discussed in the main text.

We claim in the main text that the joint inversion of phase and group velocities improves the vertical resolution of the estimated shear velocity model. This is because the sensitivity kernels of short period group velocities compress into the upper lithosphere while the long period phase velocities provide better deep sensitivity than the group velocities. Figure 4 shows an example of an inversion at a point in the Central Pacific, demonstrating this effect. The ensemble of acceptable models that fit both the phase and group velocities is substantially narrower than the ensembles that fit either wave type alone.

We also assert in the main text that the principal trends in seismic velocities and temperatures are revealed in both the seismic and thermal parameterizations. In the main text, we show results using the temperature parameterization based on a thermal model only. Figures 5 and 6 here display aspects of the 3-D seismic and temperature models estimated with the seismic parameterization. These figures are to be contrasted with Figures 2a-c, 3a-c, and 4 in the main text. Although there

are subtle differences between the seismic and temperature models that are estimated with these two different parameterizations, the general features, which are what we interpret in the main text, are very similar, particularly the trend of apparent thermal age shown in Figure 4 in the main text. We estimate apparent thermal age from the seismic parameterization by converting V_s to temperature and fitting the thermal model shown in Figure 1a in the main text to the temperature profile. This results in a range of apparent thermal age (τ) and potential temperature (T_p) estimates that define the ensemble of acceptable temperature models. To construct Figure 6 we use the middle of the ensemble.

In the main text we note that the reheating inferred in the Central Pacific is absent in the lithosphere beneath other oceans. Figure 7 shows the average temperature structure beneath the other oceans world-wide where there are lithospheric age estimates[1]. The isotherms are not observed to flatten between 70-100 Ma, in contrast with the temperature structure of the Pacific lithosphere shown in Figure 3d in the main text. The processes that reheat the lithosphere in the Central Pacific have not affected the lithosphere beneath other oceans similarly, at least not in the age range between 70-100 Ma.

Finally, Figure 8a shows the temperature profile from the 3-D convection simulation of thermal boundary layer instabilities (TBI) that is used to compute the thick solid line in Figure 4 of the main text. The heating of the lithosphere by the TBI is seen in the divergence of the isotherms from the predictions of the HSC model. The difference between lithospheric thermal structure in the TBI simulation and the HSC model is shown in Figure 8b, illustrating how TBI heats the lithosphere and cools the asthenosphere.

References

1. Mueller, R.D., W.R. Roest, J.-Y. Royer, L.M. Gahagan, and J.G. Sclater, Digital isochrons of the world's ocean floor, *J. Geophys. Res., 102*, 3211-3214, 1997.

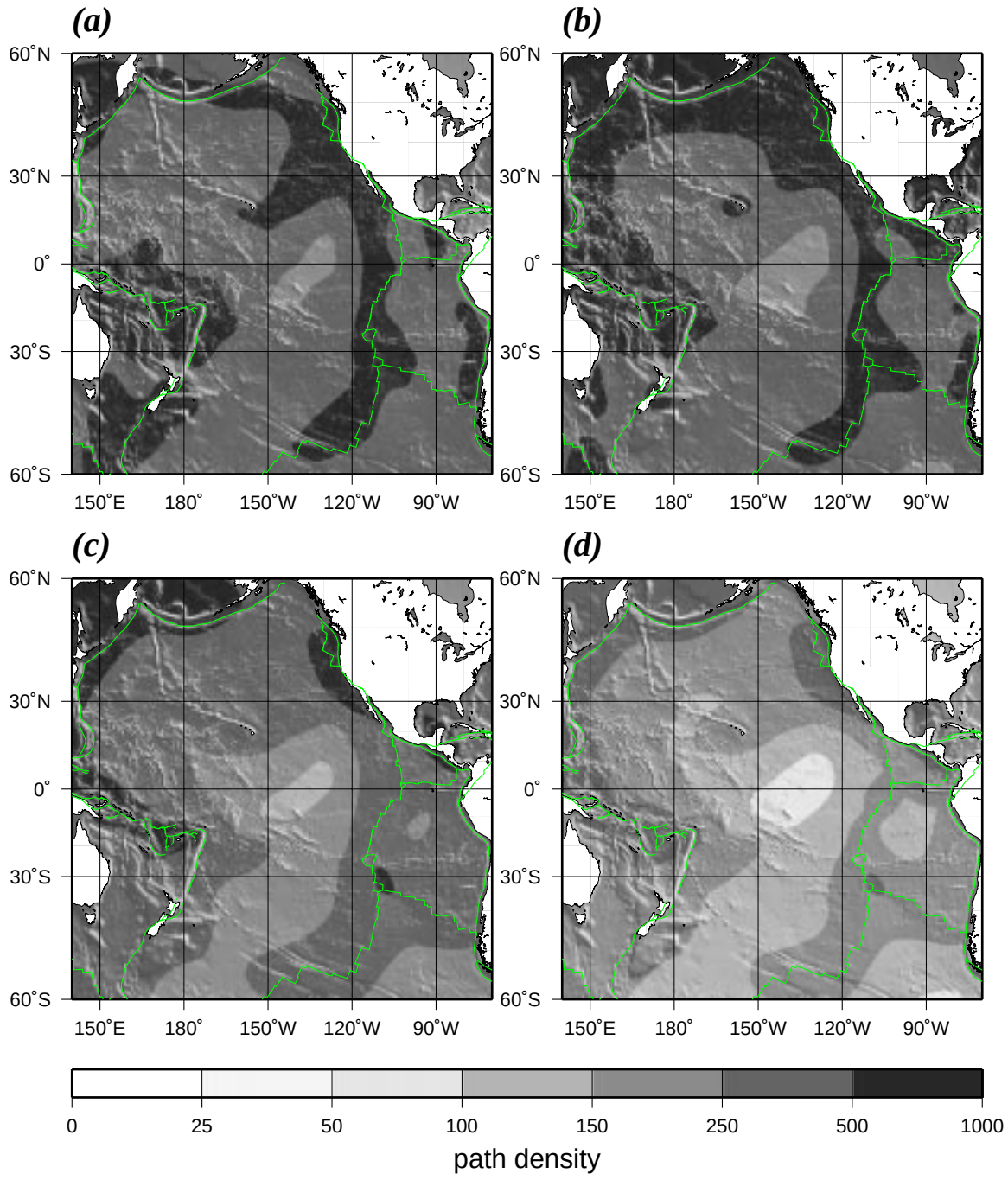

Figure 1: **Path density across the Pacific.** Path density for oceanic areas centered on the Pacific for the (a) 20 sec, (b) 50 sec, (c) 100 sec, and (d) 150 sec Rayleigh wave group velocity measurements. Path density is defined as the number of measurement paths intersecting each $2° \times 2°$ cell ($\sim$50,000 km^2). Green lines denote plate boundaries.

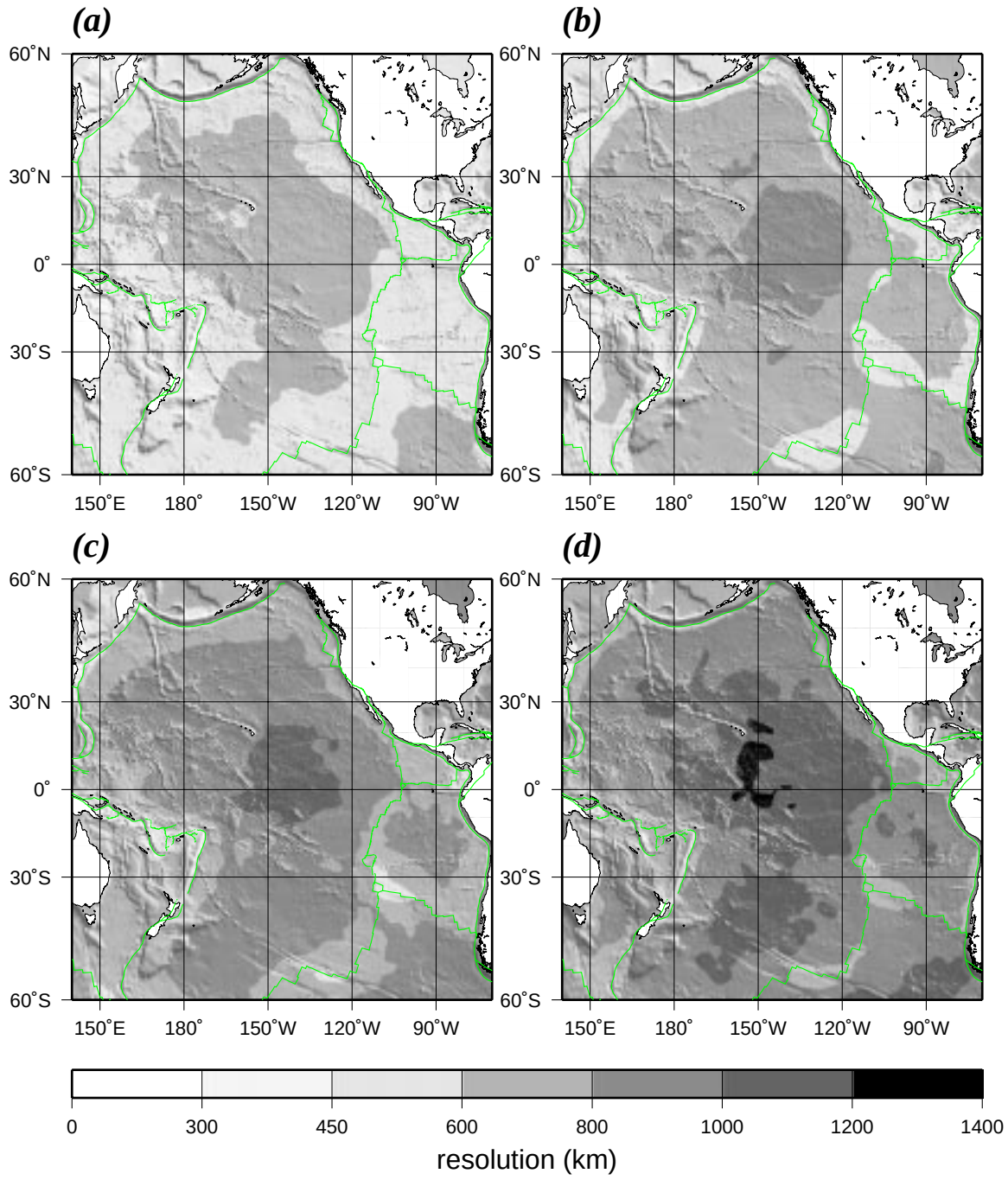

Figure 2: **Resolution estimates across the Pacific.** Resolution is estimated as twice the standard deviation of a surface Gaussian fit to the resolution surface at each point. Results here are for Rayleigh wave group velocities at periods of (a) 20 sec, (b) 50 sec, (c) 100 sec, and (d) 150 sec. Green lines denote plate boundaries.

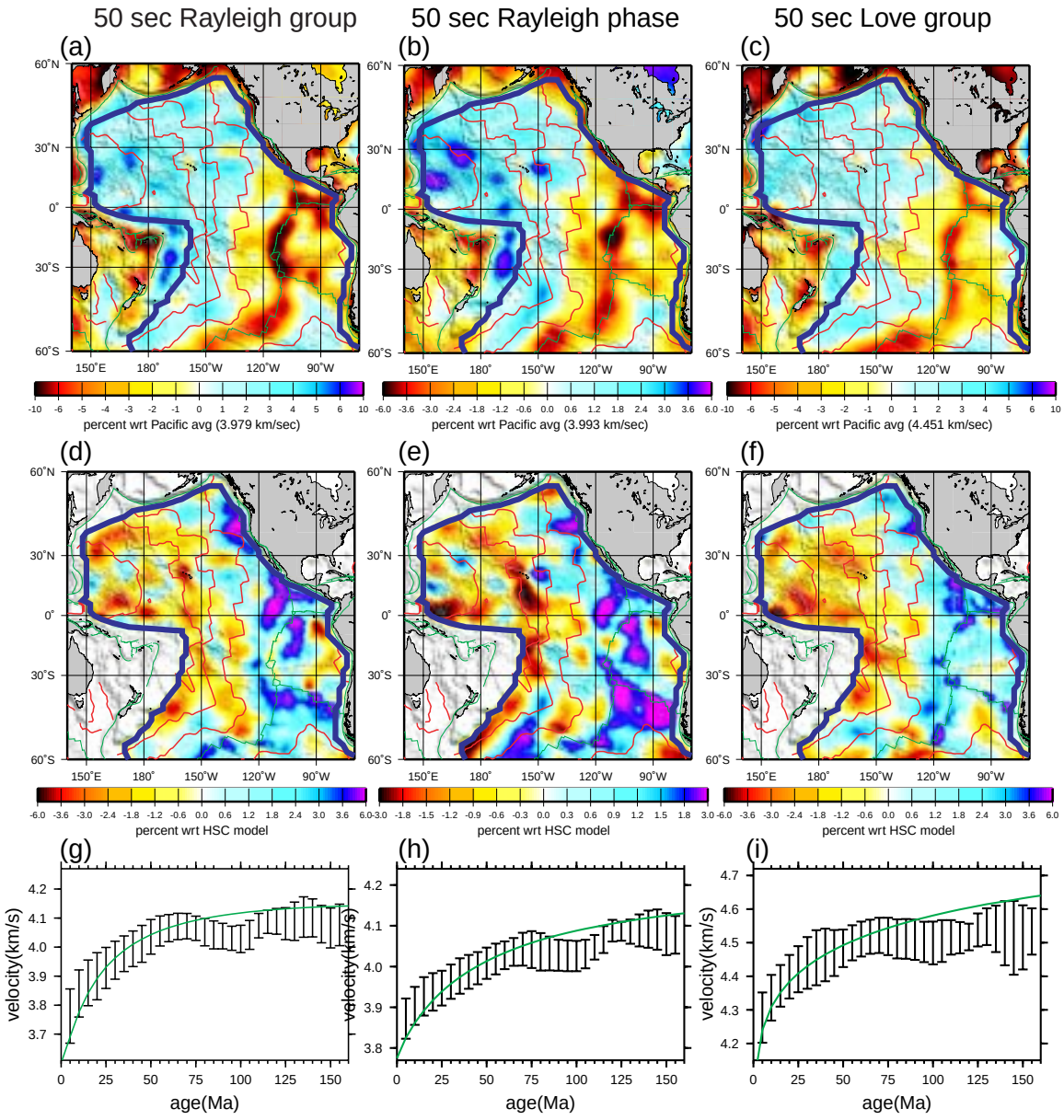

Figure 3: **Examples of 50 sec dispersion maps across the Pacific.** (a) - (c) Dispersion maps plotted as a percent perturbation to the average across the Pacific for Rayleigh group velocities, Rayleigh phase velocities, and Love group velocities, respectively. The green lines denote plate boundaries, the red lines are isochrons of lithospheric age in increments of 35 Ma, and the blue contour encloses the region where there are lithospheric age estimates. (d) - (f) Dispersion maps plotted as a percent perturbation to the prediction from the HSC model. (g) - (i) Surface wave velocities, averaged in 5 Ma lithospheric age bins across the Pacific, are plotted versus lithospheric age. Error bars represent the standard deviation within each age range. The continuous green lines are the predictions from the HSC model shifted vertically to fit the observations optimally between 10 Ma and 60 Ma: -50 m/s for Rayleigh group, -80 m/s for Rayleigh phase, and 10 m/s for Love group. The vertical shift accommodates radial anisotropy and arbitrary choices in the definition of the HSC model (e.g., initial mantle temperature).

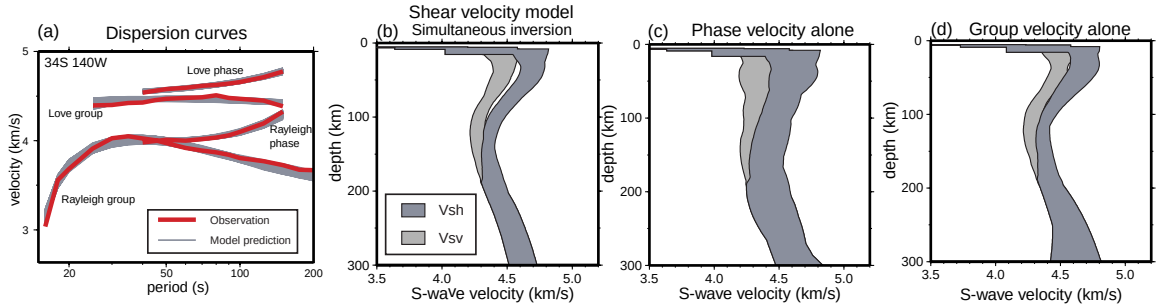

Figure 4: **Demonstration of the effect of jointly inverting phase and group velocities for a point in the Pacific (34°S, 140°W).** (a) Observed dispersion curves are plotted as the thick red line and dispersion curves from the ensemble of acceptable models shown in (b) are plotted as grey lines. (b) Corridors defined by the ensemble of acceptable models that fit group and phase velocities simultaneously. (c) Same as (b), but only phase velocities are used in the inversion. (d) Same as (b), but only group velocities are used in the inversion. Simultaneous inversion of group and phase velocities significantly improves the vertical resolution of the model.

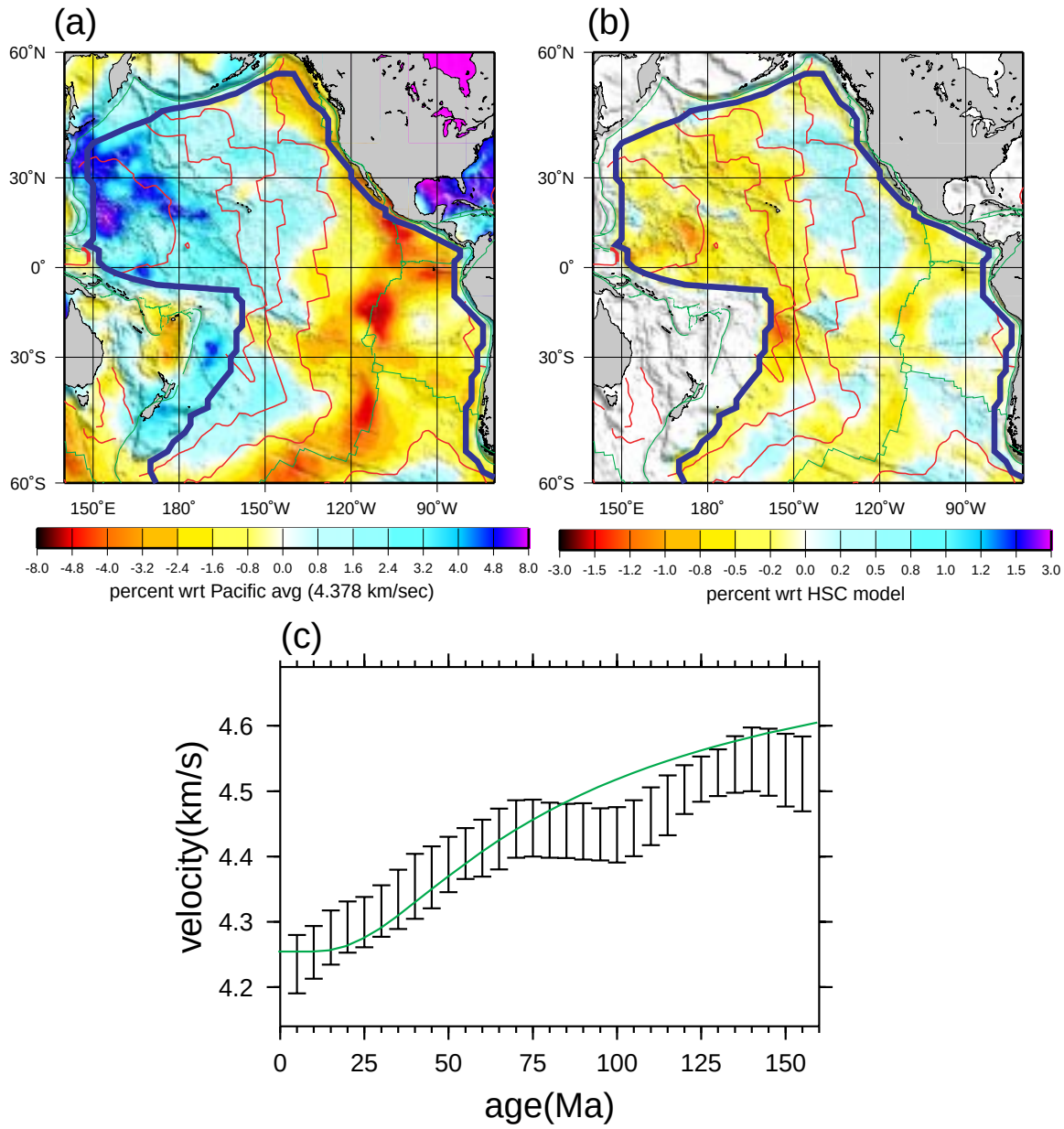

Figure 5: **Shear velocity structure of the Pacific upper mantle using the seismic parameterization and trend with lithospheric age.** (a) Isotropic shear velocity, V_s, at 100 km depth, as a perturbation to the average at this depth across the Pacific (4.378 km/sec). The green lines denote plate boundaries, the red lines are isochrons of lithospheric age in increments of 35 Ma, and the blue contour encloses the region where there are lithospheric age estimates[1]. (b) V_s at 100 km depth presented as a perturbation to the prediction from the HSC model. (c) Shear velocity, averaged in 5 Ma lithospheric age bins across the Pacific, is plotted versus lithospheric age at 100 km depth. Error bars represent the standard deviation within each age range. The continuous green lines are the predictions from the HSC model shifted vertically the same amount as in the analogous figure in the main text: -30 m/s. This figure should be contrasted with the model derived using the temperature parameterization, Figure 3a-c in the main text.

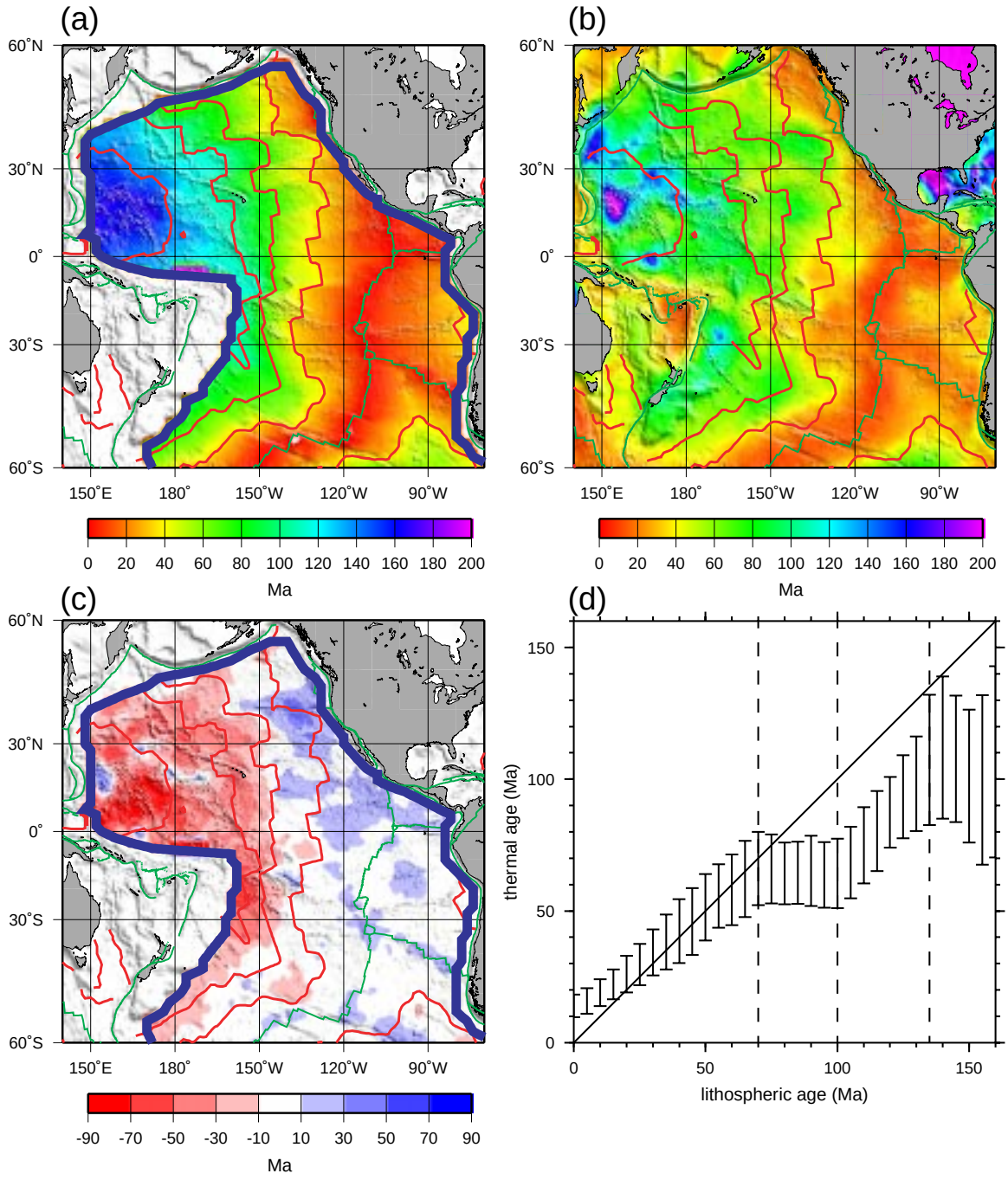

Figure 6: **Thermal age and age trend determined with the seismic parameterization.** (a) Lithospheric age in Ma, presented as a reference[1]. (b) Apparent thermal age, τ, estimated with the seismic parameterization. (c) Difference between the lithospheric age and the apparent thermal age. Reds denote that the apparent thermal age is younger than the lithospheric age. In (a) and (b), the green, red, and blue lines are as in Figure 2a-2f. (d) Comparison between apparent thermal age and lithospheric age. Apparent thermal age is averaged in 5 Ma lithospheric age bins across the Pacific and error bars represent the standard deviation within each age range. Contrast with Figures 3a-c and Figure 4 in the main text, based on the thermal parameterization.

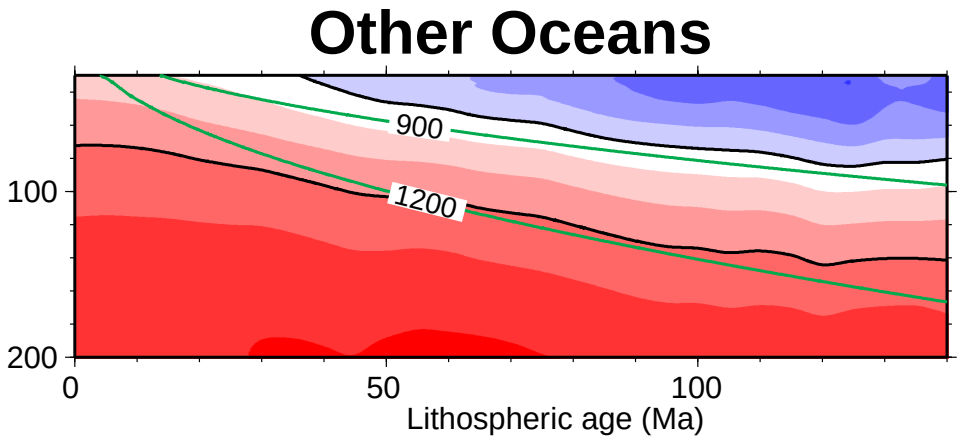

Figure 7: **Temperature in ceans other than the Pacific.** Upper mantle temperature averaged across all oceans other than the Pacific, plotted versus lithospheric age. Contrast Figure 3c in the main text. The green lines are isotherms from the HSC model.

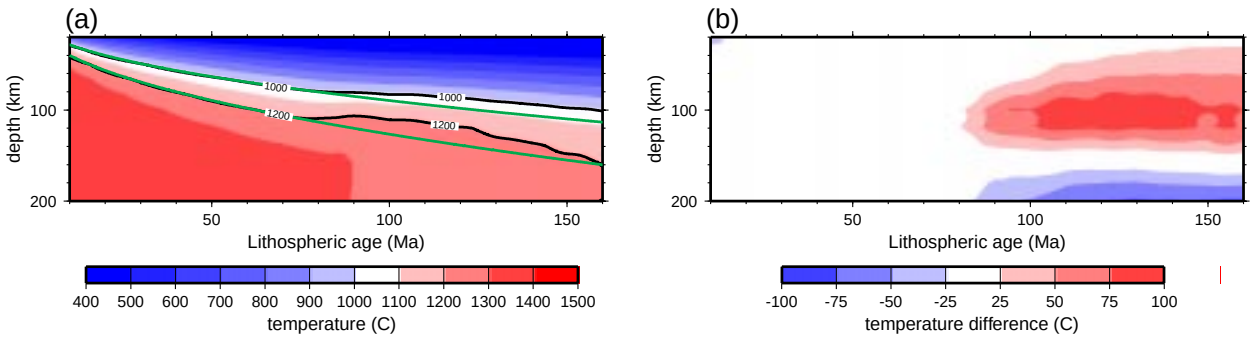

Figure 8: **Thermal structure versus lithospheric age for the simulation of TBI.** (a) Temperatures from the 3-D convection simulation of thermal boundary layer instabilities are averaged parallel to the ridge at each depth and plotted versus lithospheric age. The green lines are isotherms from the HSC model. (b) The difference between the temperatures from the simulation of TBI with the HSC model. Reds imply that temperatures in TBI simulation are warmer than in the HSC model.